Finite element simulation of 3D mechanical behaviour of NiTi shape memory alloys

Gérard Rio, Pierre-Yves Manach, Denis Favier

Arch. Mech., 47, 3, pp. 537–556, Warszawa 1995

Finite element simulation of 3D mechanical behaviour of NiTi shape memory alloys (*)

G. RIO, P. Y. MANACH (GUIDEL) and D. FAVIER (GRENOBLE)

A THREE-DEVELOPED finite element model of the isothermal deformation of shape memory alloys has been used in order to analyze and predict the mechanical behaviour of NiTi alloys. A general 3D kinematics has been studied. The constitutive behaviour is written using an elastohysteresis tensorial scheme; it is based on the splitting of the Cauchy stress tensor into two fundamental stress contributions of hyperelastic and pure hysteresis types, respectively. The equilibrium equations are then discretized by the finite element method. The validity of this formulation is established in the case of three-dimensional plate bending behaviour of NiTi shape memory alloys.

Notations

$(O, \mathbf{I}_a)$ orthonormal fixed reference frame ($a = 1,2,3$),
t absolute time,
$\partial/\partial t$ partial derivative with respect to time,
M material point,
θ^i curvilinear convected material coordinates ($i = 1,2,3$),
$\mathbf{M}$ position of point M,
$\mathbf{G}_i$ initial reference frame associated with the θ^i,
G_{ij} initial covariant components of the metric tensor $\mathbf{G}$,
$\mathbf{g}_i$ current reference frame associated with the θ^i,
g_{ij} current covariant components of the metric tensor $\mathbf{G}$,
$\sqrt{g}$ current density of metric volume per unit of material volume with $g = \det|g_{ij}|$,
$\mathbf{D}$ strain rate tensor ($2D_{ij} = \partial g_{ij}/\partial t$),
$\overline{\mathbf{D}}$ deviatoric part of the strain rate tensor,
t_r inversion time associated with an inversion point,
${}^{t}_{r}..\mathbf{G}$ Cauchy strain tensor ${}^{t}_{r}..\mathbf{G} = G_{ij}(t_r)\,\mathbf{g}^i \otimes \mathbf{g}^j$,
$\Delta^t_r..\boldsymbol{\varepsilon}$ Almansi strain tensor $\Delta^t_r..\boldsymbol{\varepsilon} = \Delta\boldsymbol{\varepsilon} = 1/2\,(\mathbf{G} - ..\,{}^{t}_{r}\mathbf{G})$,
$\overline{\boldsymbol{\varepsilon}}$ deviatoric part of the Almansi strain tensor,
$\boldsymbol{\sigma}$ Cauchy stress tensor,
$\mathbf{S}, \Delta^t_r\mathbf{S}$ deviatoric part of $\boldsymbol{\sigma}$ and of its variation,
$\mathbf{I}_{\varepsilon}, \overline{\mathbf{II}}_{\overline{\varepsilon}}, \overline{\mathbf{III}}_{\overline{\varepsilon}}$ invariants used for strain tensors: ε^i_i, $1/2\,\overline{\varepsilon}^i_j\overline{\varepsilon}^j_i$, $1/3\,\overline{\varepsilon}^i_j\overline{\varepsilon}^j_k\overline{\varepsilon}^k_i$, respectively,
E internal energy density,
$\overline{\phi}$ intrinsic dissipation rate,
W help function,
S_0, Q_0 von Mises parameters (limit shear stress S_0 and radius $Q_0 = \sqrt{2}S_0$, of the von Mises cylinder),
φ_r interpolation functions,
δ Kronecker symbol,
ω Masing functional ($\omega = 1$ or 2).

(*) Paper presented at 30th Polish Solid Mechanics Conference, Zakopane, September 5–9, 1994.

1. Introduction

THE SHAPE MEMORY ALLOY (SMA) specific properties lead to many projects of industrial applications such as, for example, electrical and mechanical connections or thermal regulation [1, 2]. However, most of these projects did not succeed due to several metallurgical and mechanical reasons. Among these reasons, the fact that no numerical tool (such as Computer Assisted Design (CAD) programs) adapted to these materials exists is an important obstacle to their industrial development. Thus, even if SMA crystallographic structure and microscopic properties (i.e. the martensitic transformation and related phenomena) have been extensively studied, it becomes essential to deepen the modelling of their thermomechanical behaviour and then to propose a numerical formulation of this behaviour adapted to an integration into CAD programs.

Up to now several authors have intended to model the thermomechanical behaviour of SMA. Some of these models are monodimensional ones [3–6] and are indeed devoided of interest to model the deformation behaviour of three-dimensional bodies. At the same time several theoretical tensorial schemes have also been developed [7–9] but as far as we know, none of these constitutive laws resulted in industrial programs or applications; for example, the program recently developed by BRINSON *et al.* [10] takes into account only monodimensional effects.

This paper is devoted to a three-dimensional finite element model of the isothermal deformation of SMA, in order to analyze and predict the mechanical behaviour of NiTi alloys. The formulation of this model is developed for large geometrical transformations including large deformations. In this context, a general 3D kinematics has been studied. The constitutive behaviour is defined using an elastohysteresis tensorial scheme which is based on the splitting of the Cauchy stress tensor into two fundamental stress contributions of hyperelastic and pure hysteresis types, respectively. Such a constitutive law has already shown its applicability for SMA [11–13]. The equilibrium equations are then deduced using the principle of virtual power, the system of nonlinear algebraic equations being solved by the Newton–Raphson method.

In a second part, the modelling ability of this formulation is presented in the case of three-dimensional plate made of NiTi shape memory alloys under bending. We focus at first on the influence of several boundary conditions on the simulation of NiTi plate bending. A set of numerical data is then displayed and compared with some simple elastic theoretical results found in the literature. Secondly, a simulation of the typical isothermal behaviours of shape memory alloys (i.e. pseudoelasticity and rubber-like behaviour) of a simple 3D body subjected to bending is proposed. This gives the first approach to the thermomechanical behaviour modelling of industrial shape memory alloy bodies.

2. Theoretical formulation

The theoretical formulation of the model is written considering large geometrical transformations including large deformations. As it was previously mentioned, a general 3D kinematics has been studied, no particular direction being favoured. Such a formulation allows for example the study of mechanical cylindric connections made of NiTi SMA. The definition of this kinematics in terms of involvements in the finite element program is briefly detailed in this paper.

2.1. Three-dimensional kinematics

Due to the incremental character of plastic constitutive laws, the description of elastoplastic deformation process is performed using an updated Lagrangian scheme, i.e. the configuration of the material at time t is taken as reference configuration for the time interval $[t, t + \Delta t]$. At the end of the increment Δt, the configuration of the material and the boundary conditions are updated, the new configuration being chosen as reference configuration for the next time increment. Let us consider a body Ω, its configuration at time t being the reference configuration. The equilibrium conditions are written in the final configuration, i.e. at

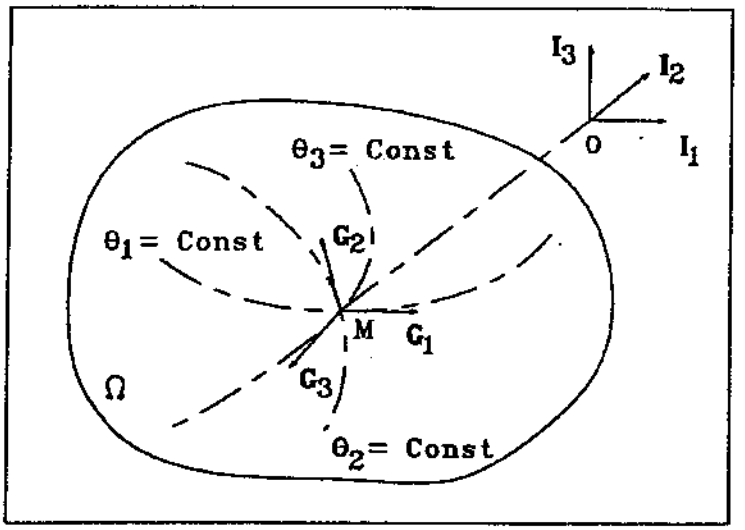

FIG. 1. Three-dimensional kinematics: definition of the convected material coordinates and of the local natural frame G_i.

time $t + \Delta t$. The position of the body Ω, see Fig. 1, is defined using convected material coordinates θ^i, so that at time t, its position can be written as

$$\mathbf{M}(\theta^i, t) = z^a(\theta^i, t)\,\mathbf{I}_a, \tag{2.1}$$

where the $\mathbf{I}_a$ vectors denote a fixed reference frame. The local frame $(M, \mathbf{G}_i)$,

also called natural frame, is defined by the relation:

$$\mathbf{G}_i = \left(\frac{\partial \mathbf{M}}{\partial \theta^i}\right)_t = \left(\frac{\partial z^a}{\partial \theta^i}\right)_t \mathbf{I}_a . \tag{2.2}$$

In the final configuration, the position of the body Ω at time $t + \Delta t$ can be written in the form $\mathbf{M}(\theta^i, t + \Delta t) = z^a(\theta^i, t + \Delta t)\,\mathbf{I}_a$, the local frame $\mathbf{g}_i$ being then defined by

$$\mathbf{g}_i = \left(\frac{\partial \mathbf{M}}{\partial \theta^i}\right)_{t+\Delta t} = \left(\frac{\partial z^a}{\partial \theta^i}\right)_{t+\Delta t} \mathbf{I}_a . \tag{2.3}$$

From these definitions, the Almansi strain tensor is written as [14, 15]

$$\Delta_t^{t+\Delta t}\varepsilon_{ij}\, \mathbf{g}^i \otimes \mathbf{g}^j = \frac{1}{2}\left(\mathbf{G} - {}_t^{t+\Delta t}..\,\mathbf{G}\right) . \tag{2.4}$$

${}_t^{t+\Delta t}..\,\mathbf{G}$ represents a tensor, the components of which are those of the metric tensor $\mathbf{G}$ in the natural frame at time t, convected without modification until the time $t + \Delta t$. Similarly, $\Delta_t^{t+\Delta t}\varepsilon_{ij}$ represents the two times covariant components of the strain tensor between times t and $t + \Delta t$. For the remaining part of this study, the strain tensor will be denoted by $\Delta\,\mathbf{e}$.

For sake of simplicity, the map of material coordinate is taken as the map of coordinate of the finite element discretization [16]. Practically, this choice imposes that the global integrals of volume should be divided into a sum of integrals performed on each element; this choice is in fact natural in the case of the finite element method.

Discretization of the kinematic fields. Let M be a material point of the body Ω. Its current position is defined by the relation:

$$\mathbf{M} = z^a\, \mathbf{I}_a = z^{ar}\, \varphi_r\, \mathbf{I}_a , \tag{2.5}$$

where the interpolation functions φ_r depend on a coordinate map ξ_i on the reference element, i.e. $\varphi_r = \varphi_r(\xi_i)$. Since the elements are assumed to be isoparametric $\varphi_r = \psi_r$ (ψ_r represents the interpolation of the functions), the displacement field $\Delta\mathbf{u}$ between times t and $t + \Delta t$ may be written as:

$$\Delta\mathbf{u} = \Delta u^a\, \mathbf{I}_a = \Delta u^{as}\, \psi_s\, \mathbf{I}_a . \tag{2.6}$$

The choice $\xi_i = \theta_i$ implies that ξ_i corresponds to the material coordinate of each element.

2.2. Constitutive behaviour

The thermomechanical behaviour of the alloys with shape-memory properties is the result of the action at a microscopical scale of reversible phenomena in association with irreversible phenomena; the observable effect of irreversible phenomena is the hysteresis loop [17] which can be universally spotted in many fields of physics [18]. Such an observation is the starting point to elaborate a class of thermomechanical schemes called elastohysteresis [11].

For SMA, the permanence of the simultaneous existence of reversible processes and hysteresis suggests to express the Cauchy stress tensor σ as the addition of two partial stresses, the first one being hyperelastic σ_r [11], while the second one is related to hysteresis of elastoplastic type σ_h [19, 20, 21]. This approach leads to the studies of two tensorial schemes of isothermal hyperelasticity and hysteresic behaviour, respectively. The last one which may be pure hysteresis (periodic under periodic loading) or evolutional hysteresis is non-standard and belongs to the discrete memory type [19, 22]. Both hyperelastic and hysteresis schemes allow the introduction of a particular formalism, the choice of which is driven by the physical processes involved in the thermomechanical behaviour of SMA. The pure elastohysteresis scheme allows the description of isothermal effects (i.e. superelasticity and pseudoelasticity) as well as shape memory effect [11].

2.2.1. Hyperelastic behaviour. For an isotropic body the hyperelastic stress is determined if one defines a density of elastic energy depending on three variables, i.e. three strain invariants. The thermomechanical properties of shape memory alloys are related to the thermoelastic martensitic transformation which occurs mainly by a shear-like mechanism. Macroscopically, if the material is assumed isotropic, the choice of the intensity of the deviatoric strain $\overline{\mathrm{II}}_{\bar{\varepsilon}}$ as the first variable of the density of elastic energy, is thus physically meaningful [11, 12]. The set of variables is completed by the ratio of elementary material volumes v and by the phase of the deviatoric strain tensor $\varphi_{\bar{\varepsilon}}$. Let us denote by $g = \det |\, g_{ij} \,|$ and $G = \det |\, G_{ij} \,|$, the ratio of elementary volumes is then defined by the relation $v = (g/G)^{1/2}$. Denoting by $\bar{\varepsilon}$ the deviatoric part of the Almansi strain tensor defined between the initial neutral state and the current state, the last variable can be expressed as:

$$\cos 3\varphi_{\bar{\varepsilon}} = 3\sqrt{6}\,\frac{\overline{\mathrm{III}}_{\bar{\varepsilon}}}{2\overline{\mathrm{II}}_{\bar{\varepsilon}}^{3/2}}, \tag{2.7}$$

where $\overline{\mathrm{III}}_{\bar{\varepsilon}}$ denotes the third invariant of the deviatoric strain tensor.

Let E be the density of elastic energy. The reversible stress contribution σ_r is defined, for an isothermal evolution, by the rate form

$$\frac{\partial E}{\partial t} = \sigma_r^{ij} D_{ji}. \tag{2.8}$$

D denotes the strain rate tensor for which $2D_{ij} = \partial g_{ij}/\partial t$ and in the isothermal case, E is simply the Helmholtz free energy. One obtains then by identifying all terms [11]:

$$\boldsymbol{\sigma}_r = \alpha_0 \mathbf{g} + \alpha_1 \Delta_0^t \boldsymbol{\varepsilon} + \alpha_2 \Delta_0^t \boldsymbol{\varepsilon} \cdot \Delta_0^t \boldsymbol{\varepsilon}, \tag{2.9}$$

where the coefficients α_i are functions of $v, \overline{\Pi}_{\bar{\varepsilon}}, \varphi_{\bar{\varepsilon}}, \partial E/\partial v, \partial E/\partial \overline{\Pi}_{\bar{\varepsilon}}$ and $\partial E/\partial \varphi_{\bar{\varepsilon}}$. In the case of shape memory alloys, a simple form for E is chosen as follows [11, 12]:

$$E = \frac{k_r \ln^2 v}{6} + \frac{Q_r^2}{2\mu_r} \ln\left[\cosh\left(\frac{2\mu_r}{Q_r}\sqrt{2\overline{\Pi}_{\bar{\varepsilon}}}\right)\right] + 2\mu_\infty \overline{\Pi}_{\bar{\varepsilon}}, \tag{2.10}$$

where k_r, Q_r, μ_r and μ_∞ are the parameters of this law and depend on the alloy and on the temperature. At this step, the variation of the hyperelastic constitutive law is needed to calculate the stiffness matrix; but for sake of clarity, the variation of strain and metric tensors, natural frame vectors as well as the variation of this law with respect to the degrees of freedom will not be detailed in this paper.

2.2.2. Pure hysteresis behaviour. The hysteresis contribution has the property of being always irreversible as it is related to the intervention of microstructural phenomena of dry friction type (strain rate-independent). It is different from a purely frictional stress due to the presence of some physical phenomena which are also able to store elastic energy. Rheological models containing elastic and slip elements have been considered to establish general pure hysteresis model [19]. From this analysis it has been shown that the internal energy and other thermomechanical quantities associated with the pure hysteresis contribution depends on the current state but also on the previous thermodynamical history through the memorisation of some discrete memory states. The material is assumed isotropic and the hysteresis contribution is only deviatoric. The basic hypotheses are the non-coupling volumetric-deviatoric behaviour and the isotropic plasticity evolution limited by the von Mises criterion which is directly included in the rate-form formulation of S; such hypotheses can be easily justified in the case of metallic materials. The constitutive law is then written in the form:

$$\frac{\partial}{\partial t}\left[\Delta_r^t S'^i_j\right] = 2\mu_h \overline{D}^i_j + \beta_4 \overline{\phi}\, \Delta_r^t S'^i_j. \tag{2.11}$$

The term $\mathbf{S}'$ is related to the deviatoric stress tensor **S** through the relation (2.14) and $\overline{\mathbf{D}}$ denotes the deviatoric strain rate tensor. The subscript r represents a reference situation which corresponds to the initial state for the first loading and to the last inversion state for the other cases, as long as any crossing point is not detected as it will be described in the next section [20]. The variable t, analogous to the time, is used to describe an evolution, and the parameter μ_h corresponds

to the Lamé's coefficient, while for a radial path, β_4 is defined by:

$$\beta_4 = -\frac{\mu_h}{\omega^2 S_0^2}, \tag{2.12}$$

where the similarity function of Masing ω is equal to 1 for the first loading and to 2 for the others. S_0 denotes the limit shear stress for the pure hysteresis contribution. The main advantage of this definition is that the identification of the parameters can be easily performed with only a tensile and a simple shear test [23]. The term $\overline{\phi}$ represents the intrinsic dissipation rate during an evolution and is defined on a radial path by the relation:

$$\overline{\phi} = \Delta_r^t S'^i_j \, \overline{D}^j_i . \tag{2.13}$$

The definition of the constitutive equation (2.11) is performed by using a mixed transportation scheme. The symmetrical components of S are obtained from those of S' by the relation:

$$S^{ij} = \frac{1}{2}\left(S'^i_k \, g^{kj} + S'^j_k \, g^{ki}\right) . \tag{2.14}$$

It can be noticed that the constitutive equation (2.11) defines the Lie derivative one time contravariant and one time covariant of the tensor S, while the previous relation can be interpreted as the integration of the Jaumann derivative of this tensor.

Resolution of the constitutive equation. The constitutive equation is a first order partial differential equation, the values of which are known at time t. It is then necessary to integrate this equation between times t and $t + \Delta t$ and two simple integration methods can be used. On the one hand, the equation can be linearized and then directly integrated by an implicit Newton method; on the other hand, it can be integrated by a Runge–Kutta explicit method [15]. In this last case, it implies that the calculation of all different values is made at several intermediate points while the first method necessitates only a calculation at time $t + \Delta t$. For the sake of simplicity and in order to be consistent with the resolution of other numerical problems (e.g. determination of inversion points), the first method has been retained here.

From these hypotheses, the derivative of S' with respect to time is linearized; denoting $\tau = t + \Delta t$, one obtains the constitutive equation in the form:

$$\frac{1}{2}\beta_4 \left[\Delta_\tau^\tau S'^l_k \, g^{km} + \Delta_\tau^\tau S'^m_k \, g^{kl}\right] \overline{D}_{lm} \, \Delta_\tau^\tau S'^i_j - \Delta_t^\tau S'^i_j + 2\mu_h \, \overline{D}^i_j = 0 \tag{2.15}$$

with

$$\Delta_t^\tau S'^i_k = \Delta_\tau^\tau S'^i_k - \Delta_\tau^t S'^i_k . \tag{2.16}$$

This equation, quadratic in $\Delta_\tau^\tau S'^i_j$, is then solved by a first order Newton method.

Determination of inversion and crossing points. The necessity of introducing discrete memory concept can be observed in the mono-dimensional case such as the one presented in Fig. 2. It can be seen in this figure that the third branch BC can not be continued along the path CD' but along the path CD which is the continuation of the first loading branch. This shows that along the path ABC, it is necessary to keep the memory of point A, memory which is erased along the path CD for after C, the behaviour is identical as if the path ABC has not been performed. Along the paths OA, then AB, BC and CD, one must keep successively the memory of points O, then O and A, then O, A and B and finally O only. Points such as A and B are called inversion points while points such as C are called crossing points.

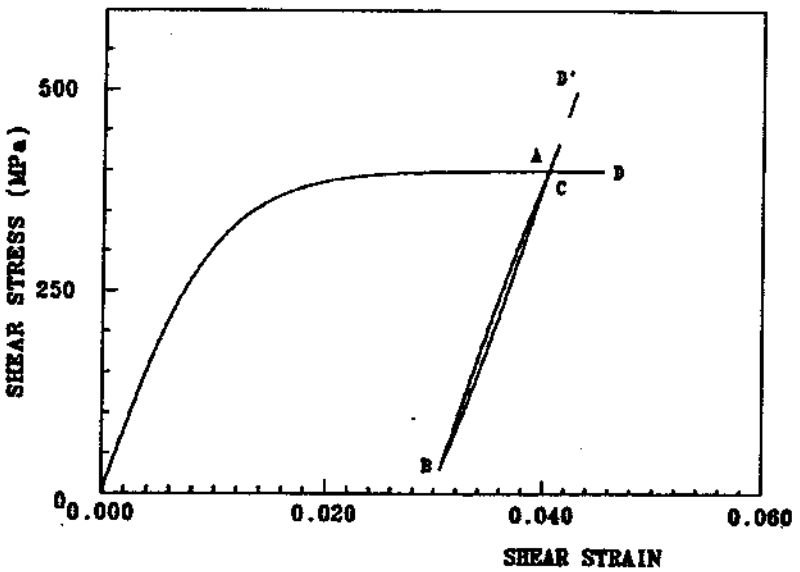

FIG. 2. Quasi-monodimensional simple shear test: definition of a pure hysteresis behaviour and of the inversion and crossing points.

The management of inversion points is performed by using the intrinsic dissipation rate function $\overline{\phi}$ presented in equation (2.13). This value is related to a volume element and must always be positive. The state at time t is an inversion point when the function $\overline{\phi}$ becomes negative. Furthermore the management of crossing points is performed by using an associate function W called help function and defined on a radial path by the relation [19, 21]:

$$W = \frac{2}{\omega^2} \int_{t_\tau}^{t} \overline{\phi}(\tau)\, d\tau \,. \tag{2.17}$$

After each inversion point, the level reached by the W function is memorized and W is set to zero for the next evolution. This function represents a measurement of dissipated energy along the path between two inversion points. A crossing

point is then observed when the current level of exchanged energy reaches a previously memorized level of W, reached on a previous branch. The crossing point represents the closure of a cycle which can then be erased. For non-radial path, the expression of relation (2.17) is rather more complicated [21]. It can be noticed that the crossing point has to be determined accurately, in order to avoid a numerical drift when performing a succession of centred cycles or loading-unloading loops.

2.3. Variational formulation

Let Ω be the region occupied by the material and Σ its boundary. The weak formulation of the boundary-value problem defined by the boundary conditions and by the equilibrium equations is obtained by using the principle of virtual power. In fact, it may be shown that this boundary-value problem is satisfied at time $t + \Delta t$ if and only if the following condition:

$$\int_{\Omega} \sigma^{ij} \; \overset{*}{v}_i |_j \, d\Omega = \int_{\Sigma} T^i \; \overset{*}{v}_i \; d\Sigma \tag{2.18}$$

is fulfilled for virtual velocity field $\overset{*}{\mathbf{v}}$ resulting from kinematically admissible displacement field. Here σ and $\mathbf{T}$ represent the Cauchy stress tensor and the surface external force, respectively. The region Ω as well as the surface Σ correspond to the material positions of the body at time $t + \Delta t$. From the finite element discretization and taking into account that the virtual velocity field is arbitrary in Ω and on Σ, this leads with (2.6) in a standard way to the system of algebraic nonlinear equations:

$$R_{bs}(\Delta u^{ar}) = 0 \qquad \forall bs, \tag{2.19}$$

where $\Delta \mathbf{u}$ denotes the displacement between time t and $t + \Delta t$, and

$$R_{bs}(\Delta u^{ar}) = \int_{\Omega(t)} \sigma^{ij} \, (\Delta u^{ar}) \; \overset{*}{v}_i |_j \, (\overset{*}{v}^{bs} = 1) \, d\Omega - \int_{\Sigma(t)} T^i \; \overset{*}{v}_i \, (\overset{*}{v}^{bs} = 1) \, d\Sigma . \tag{2.20}$$

$\overset{*}{v}^{bs}$ corresponds to the virtual velocity of a degree of freedom, $\overset{*}{\mathbf{v}}$ being chosen under the same form as the displacement field. The previous system is then solved by using the Newton–Raphson method.

3. Numerical results

This section is devoted to the numerical study of the bending behaviour of a NiTi square plate under several boundary conditions. The aim is to analyze the convergence and the ability of the elastohysteresis constitutive law to model the

pseudoelastic and the rubber-like behaviour of such shape memory alloys. The first part deals with the influence of the boundary conditions on the mechanical behaviour of a plate loaded by an uniform pressure on its upper side; then the second part deals with the influence of the mesh on the numerical results. Finally the last part is devoted to the description of the behaviour of a NiTi SMA plate in the austenitic as well as in the martensitic state.

3.1. Plate under several boundary conditions

The square plate which is studied here has the following dimensions: $40 \times 40 \times 2.6$ mm. For symmetry reasons, only the quarter of the plate, presented in Fig. 3, has been used for all tests. Therefore on faces BCGF and EFGH, the boundary conditions are symmetry type conditions, i.e. $v = 0$ on BCGF and $u = 0$ on EFGH. Three types of edge boundary conditions are used; a clamped plate (Case 1), a simply supported plate (Case 2) and a sliding simply supported plate (Case 3). For the first case, the boundary conditions are $u = v = w = 0$ on ADCB and AEHD. For the second case $w = u = 0$ on CD and $w = v = 0$ on DH, while for the last case, $w = 0$ on CD and DH. The plate is subjected to uniform pressure on the upper side ABFE. The mesh used for all these cases has 10 elements on each lateral side and 2 elements in the thickness, the elements being quadratic hexahedrons.

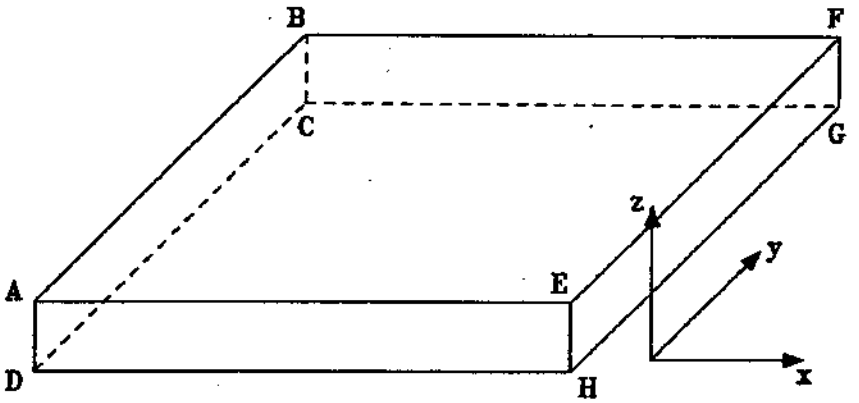

FIG. 3. Square plate used for the numerical results. u, v and w are the displacements along the x, y and z directions, respectively.

The pressure-deflection loading curves obtained for these three cases are presented in Fig. 4. The parameters of the elastohysteresis constitutive law are those determined from experimental results and given in Table 1 of the subsection 3.3. The curves drawn in dashed lines represent the simulation of respective problems with particular boundary conditions for a linear elastic material, with the Young modulus $E = 83000$ MPa and the Poisson's ratio $\nu = 0.393$; these parameters have been determined from those in Table 1 so that the associated linear

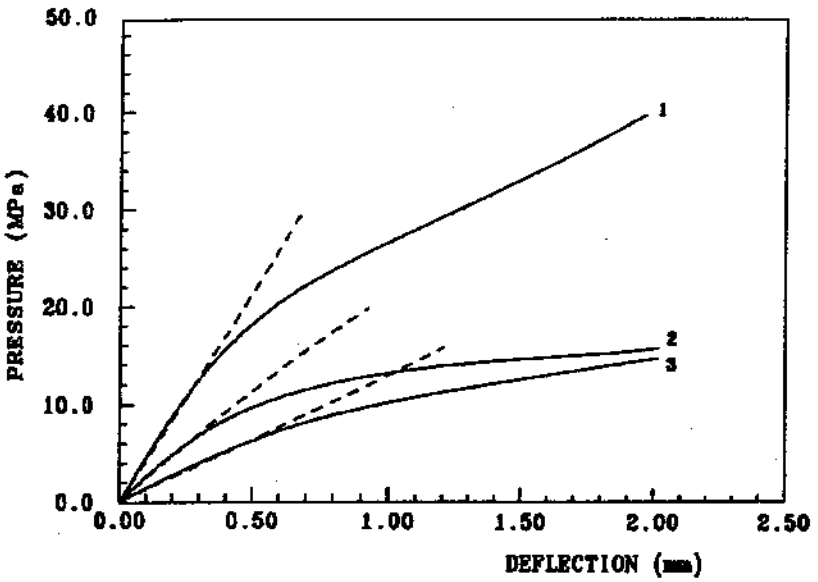

FIG. 4. Pressure-deflection loading curves obtained for a clamped plate (1), a simply supported plate (2), and a sliding simply supported plate (3). The curves in dashed line represent the elastic results associated to each case of boundary conditions with the parameters $E = 83000$ MPa and $\nu = 0.393$.

behaviour coincides with the initial quasi-linear stress-strain relation of the elastohysteresis behaviour. These elastic results have been compared to the analytical solutions given by TIMOSHENKO [24] and, despite the fact that these analytical results are given for thin plates, there is a good agreement between analytical and numerical results. Moreover, the curves drawn in full lines feature a strong nonlinear behaviour and it can be observed (like in the elastic case) that the clamped plate requires a higher pressure to be deformed, while the pressure is of the same order of magnitude in the two other cases.

The curves plotted in Fig. 5 and Fig. 6 represent the stress distributions in the thickness, both for a deflection of 2 mm. The longitudinal stress σ_{yy} and shear stress σ_{yz} are presented in Fig. 5 and Fig. 6, respectively. The value of σ_{yy} is taken in the middle of the plate while σ_{yz} is taken on the symmetry side EFGH near the edge, i.e. where it reaches its highest value. It can be observed that the variation of σ_{yy} along the thickness follows a third order symmetric curve and that this value is not too different in all cases. Such a small difference is due to the fact that the deformation state in the center of the plate is identical for all cases (as the deformed shapes are the same, see Fig. 7), since this region is far from the edges. It can be expected that for an infinite plate, these three curves will merge together. Conversely, the shear stress depends strongly on the boundary conditions, the value of σ_{yz} being much higher in the case of the clamped plate compared to the other cases when the same central deflection is considered. The clamped plate having the higher stiffness, the load must be increased to

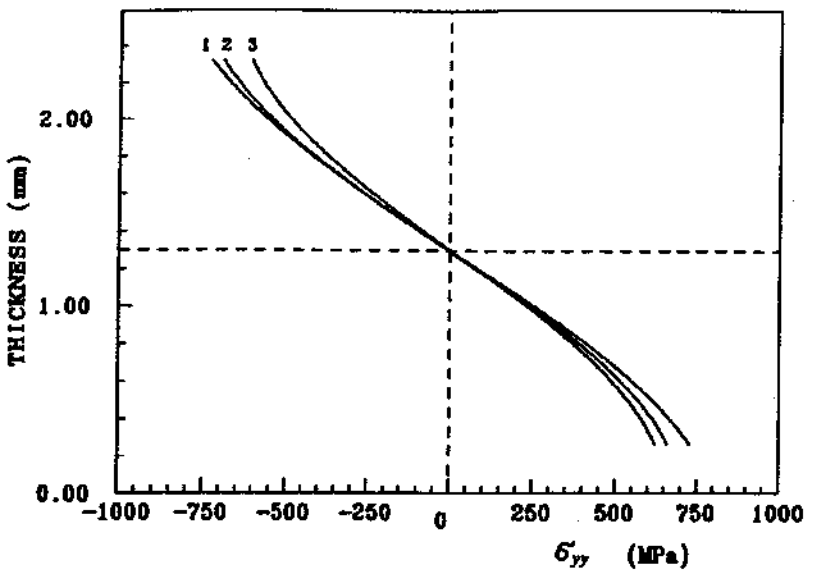

FIG. 5. Longitudinal stress distribution σ_{yy} obtained between points F and G, along the thickness for a 2 mm central deflection, for a clamped plate (1), a simply supported plate (2), and a sliding simply supported plate (3).

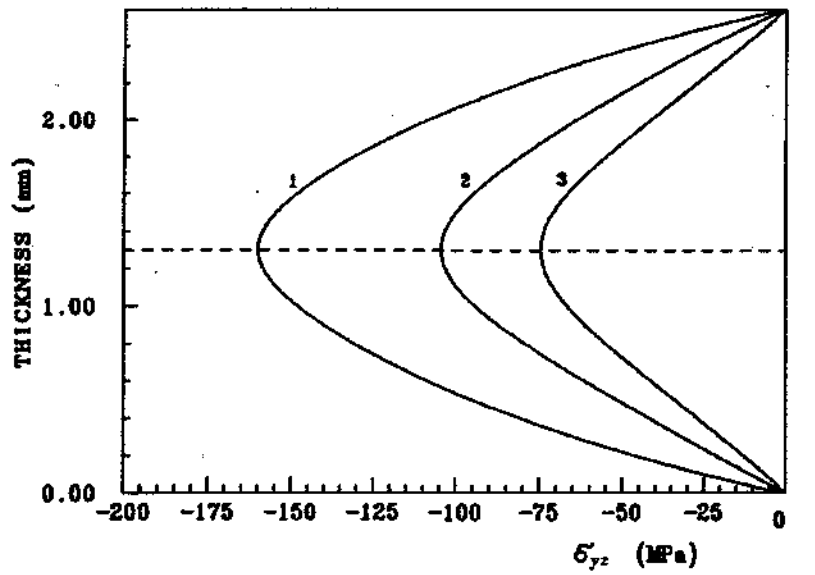

FIG. 6. Shear stress distribution σ_{yz} obtained between points E and H, along the thickness for a 2 mm central deflection, for a clamped plate (1), a simply supported plate (2), and a sliding simply supported plate (3).

obtain the same central deflection, which lead naturally to a higher shear stress level. Moreover, all curves have a classical symmetric shape with respect to the mid-plane.

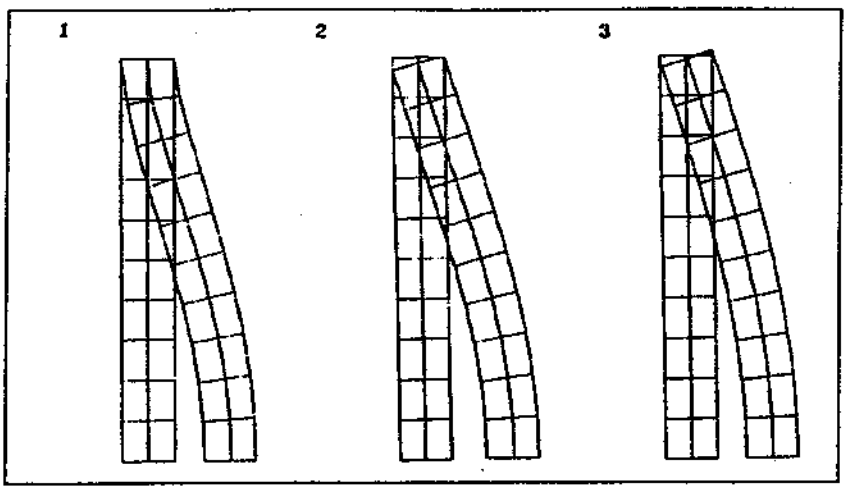

FIG. 7. Initial and deformed shape of the symmetry side EFGH of the plate for a deflection of 2 mm. Meshes correspond to a clamped plate (1), a simply supported plate (2), and a sliding simply supported plate (3).

3.2. Influence of the mesh

The influence of the mesh on the numerical results has been studied on the clamped square plate (see also subsection 3.3 for details about the material parameters). The pressure-deflection loading curves obtained for $n = 4$, 6, 8 and 10 quadratic elements on the lateral sides, respectively, are presented in Fig. 8. It can

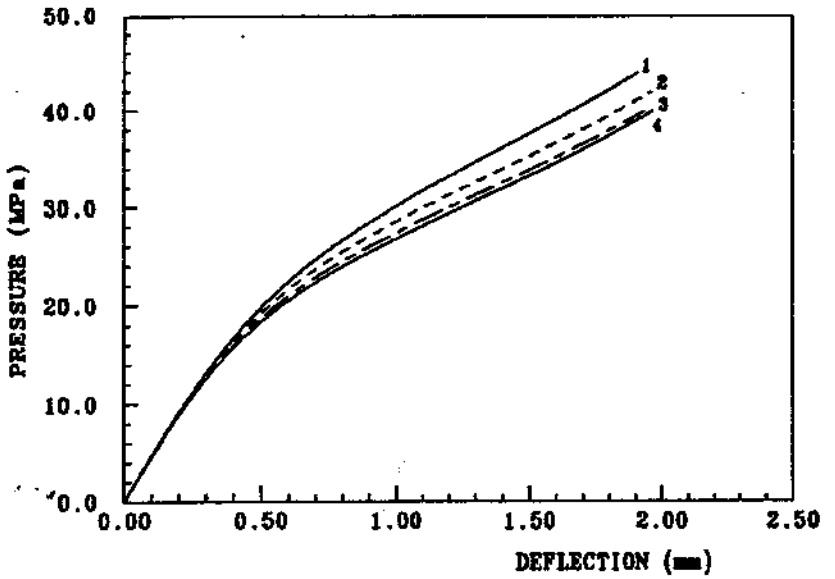

FIG. 8. Pressure-deflection loading curves obtained on a square plate for $n = 4$ (1), $n = 6$ (2), $n = 8$ (3) and $n = 10$ (4) quadratic elements on each lateral side of the plate, respectively. The mesh contains 2 elements in the thickness.

be observed that the number of elements on the edge side has a great influence on the numerical results, especially when this number is rather small. As it could be expected, a small number of elements leads to an overestimation of the bending rigidity. When this number increases, the calculations converge to a stable solution which seems to be reached for $n = 10$, for the gap between curves 3 and 4 is rather small. The curves presented in Fig. 9 represent the pressure-deflection curves obtained for $n = 1$, 2 and 3 quadratic elements in the thickness. It can be seen that for a small number of elements ($n = 1$), the rigidity of the plate is again overestimated in the range of small strains, but also that it tends to saturate for larger deformations. For a higher number of elements, the difference between curves obtained for $n = 2$ and 3 elements becomes quasi-negligible.

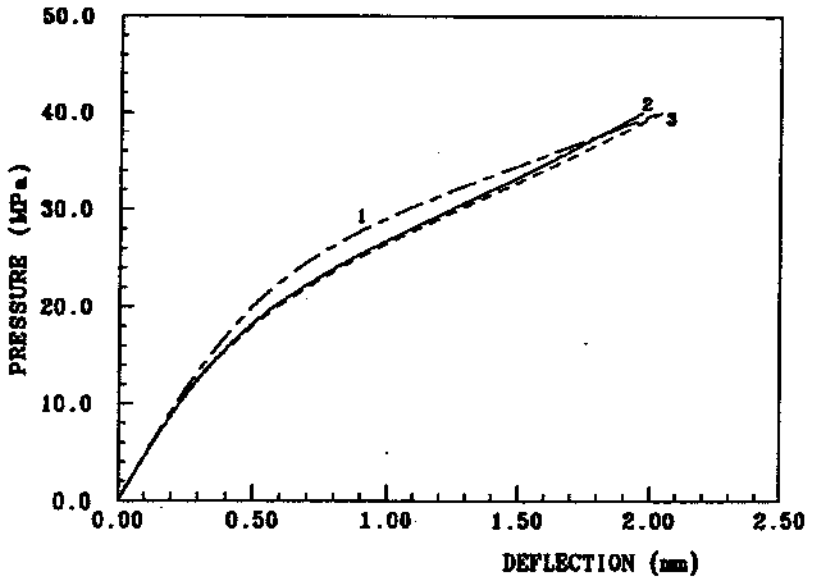

Fig. 9. Pressure-deflection loading curves obtained on a square plate for $n = 1$ (1), $n = 2$ (2) and $n = 3$ (3) quadratic elements in the thickness of the plate, respectively. The mesh contains 10 elements on each lateral side.

As a whole, a mesh of $n = 10$ elements on each lateral side and of $n = 2$ elements in the thickness offers a good compromise between the accuracy, the reliability of the mesh and the calculation time. This mesh is used for all the other calculations; indeed, one observes that the convergence is stable in all tests, no locking phenomenon appears and the solution always converges to a stable shape.

3.3. Shape memory alloy behaviour

Concerning the study of SMA, the material parameters have been identified on a NiTi alloy from the experimental results obtained in simple shear by Manach [13]. The determination of these parameters has already been detailed

in MANACH *et al.* [23]. The values are given in Table 1 (in MPa) and are considered as temperature-independent.

Table 1. Material parameters of the elastohysteresis constitutive law.

	k_r	μ_r	μ_∞	μ_h	S_0
Austenitic state	425000	22500	2500	7500	100
Martensitic state	425000	22500	2500	7500	200

The evolution of Q_r as a function of the temperature has been determined to follow a linear relation such as: $Q_r = 5\sqrt{2}(T - 313)$ MPa [23] for $T > 313$ K, and 0 MPa otherwise. In the austenitic state, the test is performed at $T = 353$ K and in the martensitic state at $T = 313$ K. The numerical simple shear stress-strain curves obtained using these parameters are presented in Fig. 10 and Fig. 11 for the austenitic and martensitic states, respectively. Moreover, loops and subloops have been performed on these simulated curves in order to feature the main characteristics of the elastohysteresis model. The results obtained on the pressure-deflection loading-unloading curves in the middle of the plate are presented in Fig. 12 in the austenitic (A) and in the martensitic (M) state, respectively.

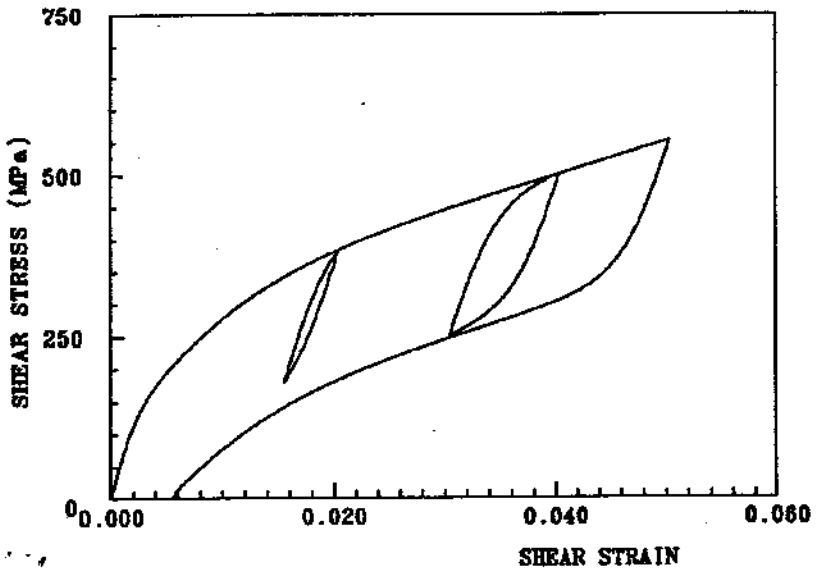

FIG. 10. Numerical stress-strain curve obtained in simple shear on a NiTi alloy from the parameters identified by the experimental results of Manach [13] in the austenitic state at $T = 353$ K.

, It is now well known that the deformation mode of materials presenting a thermoelastic martensitic transformation is highly influenced by the temperature at which the deformation takes place. Two mechanisms of deformation can

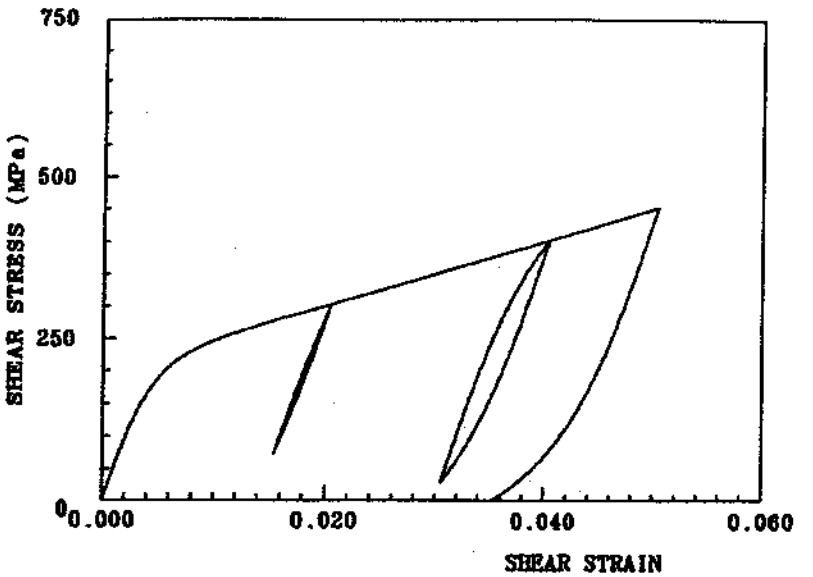

FIG. 11. Numerical stress-strain curve obtained in simple shear on a NiTi alloy from the parameters identified by the experimental results of Manach [13] in the martensitic state at $T = 313$ K.

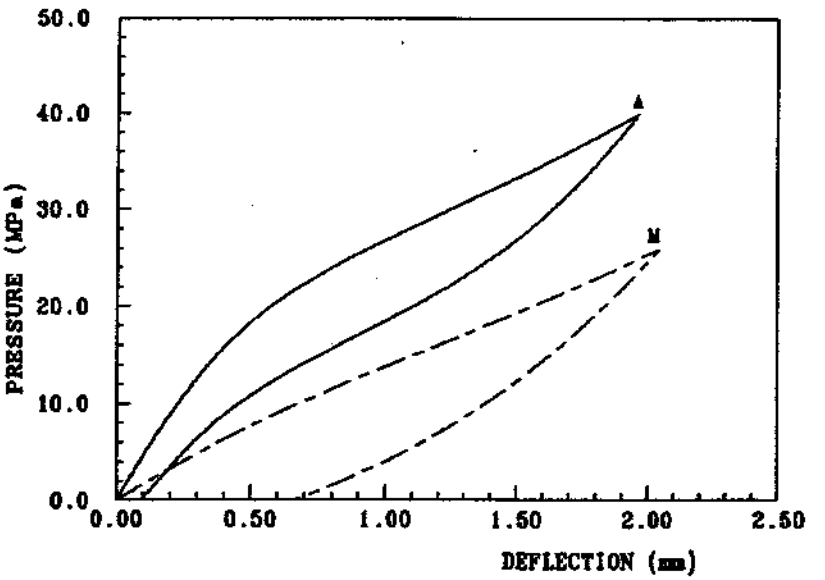

FIG. 12. Pressure-deflection loading-unloading curve obtained for the bending of a NiTi clamped square plate in the austenitic (A) and in the martensitic (M) state, respectively.

occur, i.e. the reorientation of the martensite variants when the material is in the martensitic state, and the stress-induced martensitic transformation when the

material is in the austenitic state. Qualitatively, the curves presented in Fig. 12 exhibit the typical mechanical behaviours of SMA related to these two previous phenomena, i.e. the superelastic effect of the austenitic phase and the rubber-like behaviour of the martensitic phase. Then for curve (M), the deformation is produced by the motion of internal defects such as martensite-martensite interfaces or martensite twins. The loading curve corresponds to the development of the martensite variant reorientation, while the unloading curve is characterized by a partial reorientation of the martensite variants, producing then a greater reverse deformation than the classical elastic deformation. For curve (A), the main mechanism of deformation is produced by the stress-induced martensitic transformation during loading and its quasi-total reversion during unloading, e.g. [25].

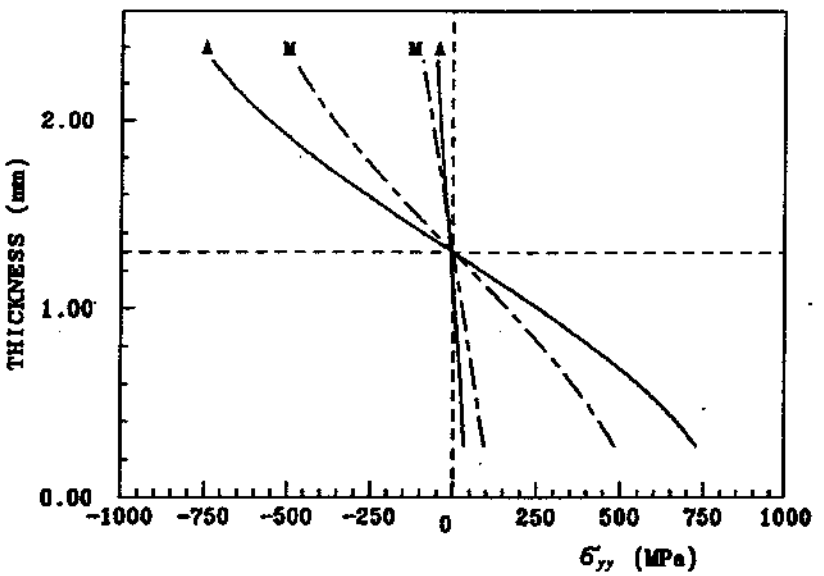

FIG. 13. Longitudinal stress distribution σ_{yy} obtained between points F and G, along the thickness, for a 2 mm central deflection, for a clamped plate at the end of the loading and unloading in the austenitic (A) and in the martensitic (M) state, respectively.

The stress distributions in the thickness are presented in Fig. 13 and Fig. 14 for the longitudinal stress σ_{yy} and for the shear stress σ_{yz}, respectively. Comparisons are made for the same central deflection of 2 mm. It can be observed that the residual stresses are of the same order of magnitude, the longitudinal stress σ_{yy} being greater in the martensitic state (which is more deformed) while the shear stress σ_{yz} is similar for both cases, which is coherent with consideration of subsection 3.1. It can also be pointed out that those stress distributions are in agreement with the analytical solutions given by Kirchhoff for an elastic clamped square plate.

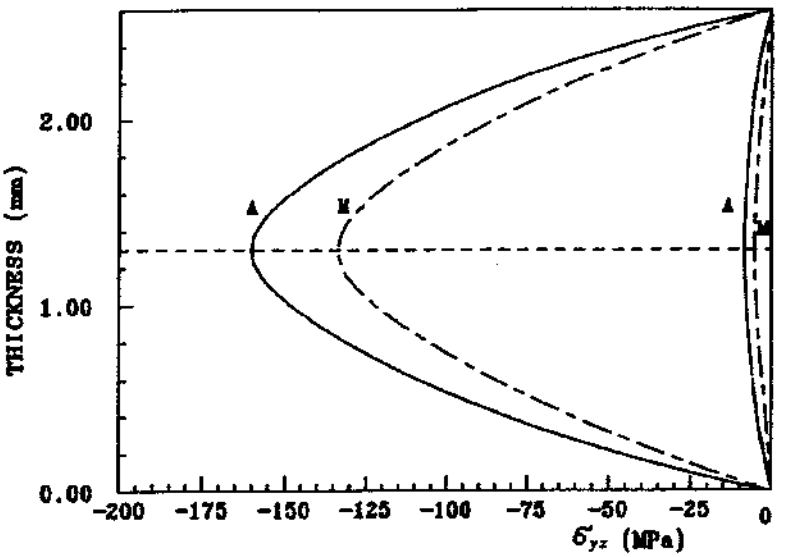

FIG. 14. Shear stress distribution σ_{yz} obtained between points E and H, along the thickness for a 2 mm central deflection, for a clamped plate at the end of the loading and unloading in the austenitic (A) and in the martensitic (M) state, respectively.

4. Conclusions

A new three-dimensional finite element model of the unusual deformation of shape memory alloys has been developed. The validity of this model has been analyzed in the case of the bending behaviour of NiTi alloy. The formulation of this model is written in the case of large geometrical transformations including large deformations. In this context, a general 3D kinematics has been studied. The constitutive behaviour is defined using an elastohysteresis tensorial scheme and finally, the equilibrium equations are deduced using the principle of virtual power which is solved by the finite element method.

The modelling ability of the formulation has been presented in the case of three-dimensional plate behaviour, the numerical study concerning the bending behaviour of a NiTi square plate under several boundary conditions. The behaviour of the plate under several boundary conditions features a good agreement, at the beginning of the loading, between the numerical and analytical elastic results, while the influence of the mesh has also been analyzed. Furthermore, this study shows that the behaviour of SMA is well modelled by the elastohysteresis constitutive law and that the main effects observed numerically are consistent with those observed experimentally on such shape memory alloys.

Acknowledgements

The authors are grateful to the Service Technique des Programmes Aéronautiques of the French Ministry of Defence for financial support. The authors also wish to thank P. GUÉLIN and P. PÉGON for useful discussions.

References

1. P. SCHMIDT-MENDE and G. BLOCK, *Applications of NiTi-based shape memory alloys*, [in:] Proc. European Conference on Martensitic Transformations in Science and Technology, p. 245, Bochum, Germany 1989.
2. D. STÖCKEL, *Industrial applications of NiTi shape memory alloys*, [in:] Proc. European Conference on Martensitic Transformations in Science and Technology, p. 223, Bochum, Germany 1989.
3. I. MÜLLER and K. WILMANSKI, *A model for phase transition in pseudoelastic bodies*, Il Nuevo Cimento, 57B, p. 283, 1980.
4. F. FALK, *Model free energy, mechanics and thermodynamics of shape memory alloys*, Acta Metall., 28, p. 1773, 1980.
5. L. LÜ, E. AERNOUDT, P. WOLLANTS, J. VAN HUMBEECK and L. DELAEY, *Simulation of transformation hysteresis*, Zeitschrift für Metallkunde, 81, p. 613, 1990.
6. J. ORTIN, *Partial hysteresis cycles in shape memory alloys: experiments and modelling*, [in:] Proc. European Symposium on Martensitic Transformation and Shape Memory Properties, p. C4-13, Aussois, France 1991.
7. K. TANAKA, S. KOBAYASHI and Y. SATO, *Thermomechanics of transformation pseudoelasticity and shape memory effect in alloys*, Intern. J. Plast., 2, p. 59, 1986.
8. E. PATOOR, A. EBERHARDT and M. BERVEILLER, *Potentiel pseudoélastique et plasticité de transformation martensitique dans les mono et polycristaux métalliques*, Acta Metall., 35, p. 2779, 1987.
9. M. FREMOND, *Mécanique des milieux continus: matériaux à mémoire de forme*, C.R. Académie des Sciences de Paris, 304, p. 239, 1987.
10. L.C. BRINSON and R. LAMMERING, *Finite element analysis of the behavior of shape memory alloys and their applications*, Intern. J. Solids and Structures, 30, p. 3261, 1993.
11. D. FAVIER, *Contribution à l'étude théorique de l'élastohystérésis à température variable: application aux propriétés de mémoire de forme*, Thèse d'Etat, Institut National Polytechnique de Grenoble, Grenoble, France, 1988.
12. D. FAVIER, P. GUÉLIN and P. PÉGON, *Thermomechanics of hysteresis effects in shape memory alloys*, [in:] Proc. Intern. Conference on Martensitic Transformation, p. 559, Sydney, Australia 1989.
13. P.Y. MANACH, *Etude du comportement thermomécanique d'alliages à mémoire de forme NiTi*, Thèse de Doctorat, Institut National Polytechnique de Grenoble, Grenoble, France 1993.
14. P. GUÉLIN, *Notes on the Cauchy tensors* $g^i \otimes g^j \, {}^t_R\sigma_{ij}$ *and* $g_i \otimes g^j \, {}^t_R\sigma^i_{\ j}$ *expressing the discrete memory concept*, [in:] Summer School in Two-phase Medium Mechanics, p. 57, Gdańsk, Poland 1983.
15. P. PÉGON and P. GUÉLIN, *Finite strain plasticity in convected frames*, Intern. J. Numerical Methods in Engng., 22, p. 521, 1986.
16. G. RIO, B. TATHI and F. HORKAY, *Introducing bending rigidity in a finite element membrane sheet metal forming model*, [in:] Proc. Intern. Seminar Mecamat'91, p. 449, Fontainebleau, France 1991.
17. H. VERGUTS, L. DELAEY, E. AERNOUDT and W. VERMEERSCH, *On hysteresis effects in shape memory alloys*, [in:] Proc. Euromech Colloquium 171, p. 214, Warszawa, Poland 1983.
18. D. FAVIER, P. GUÉLIN and R. CAMMARANO, *Application of a phenomenological elastohysteresis theory to the modelling of magnetisation*, [in:] Proc. Intern. Symposium on Magnetic Anisotropy and Coercivity in Rare-Earth Transition Metal Alloys, p. 137, Canberra, Australia 1992.
19. P. GUÉLIN, *Remarques sur l'hystérésis mécanique: les bases d'un schéma thermomécanique à structure héréditaire*, J. Mécanique, 19, p. 217, 1980.
20. B. WACK, J.M. TERRIEZ and P. GUÉLIN, *A hereditary type, discrete memory, constitutive equation with applications to simple geometries*, Acta Mech., 50, p. 9, 1983.
21. P. PÉGON, *Contribution à l'étude de l'élastohystérésis élastoplastique*, Thèse d'Etat, Institut National Polytechnique de Grenoble, Grenoble, France 1988.

22. P. PÉGON, P. GUÉLIN, D. FAVIER, B. WACK and W.K. NOWACKI, *Constitutive scheme of discrete memory form for granular materials*, Arch. Mech., 43, p. 3, 1991.

23. P.Y. MANACH and D. FAVIER, *Comparison between isothermal tensile and shear tests on a NiTi shape memory alloy*, [in:] Proc. Intern. Conference on Martensitic Transformations, p. 941, Monterey, USA, 1992.

24. S. TIMOSHENKO and S. WOINOWSKY-KRIEGER, *Théorie des plaques et des coques*, Dunod, Paris 1961.

25. S. MIYAZAKI, K. OTSUKA and Y. SUZUKI, *Transformation pseudoelasticity and deformation behavior in a Ti–50.6at %Ni alloy*, Scripta Metall., 15, p. 287, 1981.

UNIVERSITÉ DE BRETAGNE OCCIDENTALE
LABORATOIRE DE GÉNIE MÉCANIQUE ET MATÉRIAUX, GUIDEL
and
UNIVERSITÉ JOSEPH FOURIER
LABORATOIRE SOLS-SOLIDES-STRUCTURES, GRENOBLE, FRANCE.

Received November 28, 1994.